Tidal conversion and mixing poleward of the critical latitude (an Arctic case study)

Rippeth, Thomas; Vlasenko, Vasiliy; Stashchuk, Nataliya; Scannell, Brian; Green, Mattias; Lincoln, Benjamin; Bacon, Sheldon

Geophysical Research Letters

DOI:
10.1002/2017GL075310

Published: 28/12/2017

Peer reviewed version

Tidal conversion and mixing poleward of the critical latitude (an Arctic case study)

Tom P. Rippeth[1], Vasiliy Vlasenko[2], Nataliya Stashchuk[2], Brian D. Scannell[1], J. A. Mattias Green[1], Ben J. Lincoln[1], and Sheldon Bacon[3]

[1]School of Ocean Sciences, Bangor University, Bangor, LL59 5AB, UK

[2]School of Biological and Marine Sciences, Plymouth University, Plymouth, PL4 8AA, UK

[3]National Oceanography Centre, Southampton, SO14 3ZH, UK

Key Points:

- The paper focuses on a region of significant tidal conversion and supercritical Froude number flow poleward of the critical latitude.
- A numerical model is used to show that tidally generated high frequency internal waves are a key mechanism for conversion of tidal energy poleward of this latitude.
- Observations show features characteristic of high frequency internal waves, with co-incident turbulence measurements suggesting significant mixing associated with these waves.

Corresponding author: Tom P. Rippeth, t.p.rippeth@bangor.ac.uk

Abstract

The tides are a major source of the kinetic energy supporting turbulent mixing in the global oceans. The prime mechanism for the transfer of tidal energy to turbulent mixing results from the interaction between topography and stratified tidal flow, leading to the generation of freely propagating internal waves at the period of the forcing tide. However, poleward of the critical latitude (where the period of the principal tidal constituent exceeds the local inertial period), the action of the Coriolis force precludes the development of freely propagating linear internal tides. Here we focus on a region of sloping topography, poleward of the critical latitude, where there is significant conversion of tidal energy and the flow is supercritical (Froude number, Fr $>$ 1). A high-resolution non-linear modelling study demonstrates the key role of tidally generated lee waves and super-critical flow in the transfer of energy from the barotropic tide to internal waves in these high latitude regions. Time series of flow and water column structure from the region of interest show internal waves with characteristics consistent with those predicted by the model, and concurrent microstructure dissipation measurements show significant levels of mixing associated with these internal waves. The results suggest that tidally generated lee-waves are a key mechanism for the transfer of energy from the tide to turbulence poleward of the critical latitude.

1 Introduction

The tide plays a key role in global ocean circulation through the supply of mechanical energy to turbulence which stirs the ocean, promoting mixing [*Munk and Wunsch*, 1998]. There has been much recent interest in the role of the tides in driving mixing in the climatically sensitive Arctic Ocean. Microstructure measurements of the rate of dissipation of turbulent kinetic energy (ε) have indicated significantly enhanced mixing over areas of sloping topography compared to the very quiescent conditions observed elsewhere in the Arctic Ocean [e.g. *Padman and Dillon*, 1991; *D'Asaro and Morison*, 1992; *Fer et al.*, 2010; *Rainville and Winsor*, 2008]. *Rippeth et al.* [2015] show that the enhanced levels of ε observed over the Arctic Ocean continental shelf break are correlated to the rate of conversion of barotropic tidal energy. This is an interesting result given that much of the Arctic Ocean lies poleward of the critical latitude, ϕ_c, at which the local inertial period matches the period of the principal semi-diurnal tidal constituent (M2) (Figure 1). Stratified tidal flow over sloping topography can produce lee waves at any latitude. However, poleward of the critical latitude linear wave theory does not permit the generation of a freely propagating internal tide,

the widely cited pathway for tidal energy conversion to turbulence in the ocean equatorward of the critical latitude [e.g. *Green and Nycander*, 2013].

Dynamically there are two principal mechanisms for tidal energy conversion from the barotropic to baroclinic modes over sloping topography. They are distinguished by the relative contribution of the two acceleration terms in the momentum balance equation:

$$\frac{d\mathbf{v}}{dt} = \frac{\partial \mathbf{v}}{\partial t} + (\mathbf{v}\cdot\nabla)\mathbf{v} \tag{1}$$

Here $\mathbf{v}$ is the velocity vector with components u, v, and w directed along the Ox, Oy, and Oz axes, respectively, in a Cartesian coordinate system with the (xy) plane placed on the undisturbed free surface and the z-axis directed vertically upward.

In a linear approximation with an assumption of weak tidal activity when only small-amplitude waves are generated [see, e.g., *Nycander*, 2005; *Falahat and Nycander*, 2015], the second term in the right-hand side of Eq. (1) is neglected and the governing system for plane waves in an inviscid fluid is reduced to a single wave equation [*Vlasenko et al.*, 2005]:

$$w_{xx} - \frac{\sigma^2 - f^2}{N^2(z) - \sigma^2} w_{zz} = 0 \tag{2}$$

Here $f = 2\Omega\sin(\phi)$ is the Coriolis parameter, Ω is the angular frequency of the Earth's rotation, ϕ is latitude, $N(z)$ is the buoyancy frequency such that $N^2(z) = -(g/\rho)(\partial\rho/\partial z)$, where g is the acceleration due to gravity, ρ the water density, and σ is the tidal frequency.

In systems with weak rotation ($f < \sigma < N$), Eq. (2) is hyperbolic, with solutions that represent progressive internal waves of tidal frequency radiated from the source as freely propagated waves. However, in systems with strong rotation ($f > \sigma$), including latitudes poleward of ϕ_c - which is 74.5° for the semi-diurnal M2 tidal constituent - the equation becomes elliptic, and solutions represent evanescent waves decaying exponentially away from the source. Excluding the non-linear terms in Eq. (1) therefore results in a prediction that rotation will significantly reduce the conversion of energy from the barotropic tide to the baroclinic internal tide polewards of ϕ_c. However, the non-linear terms may actually contribute to tidal energy conversion through the tide-topography interaction [*Bell*, 1975; *Nakamura and Awaji*, 2000; *Nakamura et al.*, 2000]. *Vlasenko et al.* [2005] show that the advective term in Eq. (1) can lead to the generation of unsteady lee waves. The properties of these waves are very different to those of long baroclinic tidal waves, as they occur as packets of high frequency internal waves with a spatial scale of the same order as the bottom topographic features. They are generated by tidal currents on the lee side of the sloping bottom

topography. As the down slope current accelerates, the waves are trapped, forming a type of hydraulic jump. *Vlasenko et al.* [2003] suggest that this "lee jump" formation as a potential mechanism for conversion of tidal energy poleward of the critical latitude. Here we use "lee wave" to mean the structure described above, rather than propagating internal waves generated by a general (non-tidal) flow.

The aim of this paper is to demonstrate that lee wave generation coupled with supercritical barotropic tidal flow over sloping topography is potentially a key mechanism for the transfer of energy from the tide to turbulent mixing poleward of the critical latitude. To achieve this we will combine evidence from a proof of concept high resolution numerical modelling study with new in-situ observations of profiles of the rate of dissipation of turbulent kinetic energy (ε) from a region of significant tidal conversion and supercritical tidal flow poleward of the critical latitude.

2 Region of Interest

The focus of the present study is the Spitsbergen Bank, a shallow bank to the east of the Fram Strait and south of Svalbard which is poleward of the critical latitude ϕ_c (Figure 1). A 12-hour time series of measurements were made here on the 8 August 2013, a couple of days ahead of a spring tide. These measurements included profiles of water column structure, velocity and ε made at a location on the edge of the bank (75°30'; Figure 1a).

The rate of conversion of barotropic tidal energy over the region is expressed as a local balance between the rate of work done by the tide generating force and the divergence in the tidal energy flux [*Egbert and Ray*, 2001]. The rate of tidal conversion is the sum of the rates of energy transfer to baroclinic modes and to dissipation in the bottom boundary layer. Here, it is computed using tidal amplitudes and currents from the TPX08 database (available from volkov.oce.orst.edu/tides/tpx08_atlas.html). Figure 1b shows the rate of tidal energy conversion over the region of interest with high conversion rates estimated over the bank indicating that the Spitsbergen Bank is an area of significant conversion of barotropic tidal energy. The water column was stratified with warmer (6.8°C), fresher (34.53) water overlying cooler (3.5°C), saltier (34.93) water at the time of the measurements with maximum stratification between approximately 20 m and 40 m (Figure 1d).

A necessary condition for unsteady lee wave generation is that the Froude number, $Fr = U/c$, where U is the tidal velocity and c is the phase speed of internal waves, should

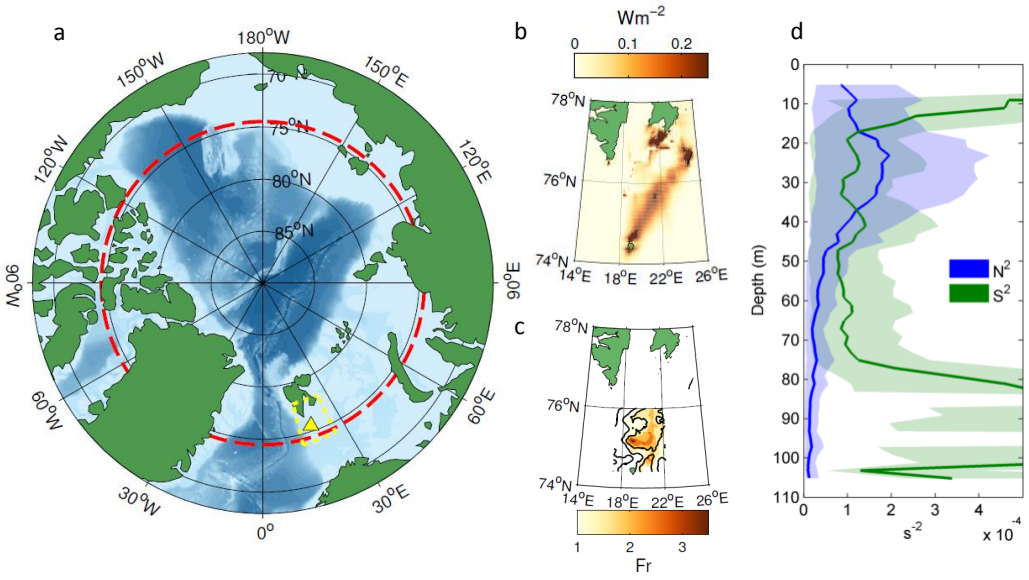

Figure 1. (a) A map of the Arctic Ocean showing the position of the observations (yellow triangle). The critical latitude at which the local inertial period matches the period of the principle semi-diurnal tidal constituent (M2) is shown as a red dashed line. Lighter blue areas indicate shallower regions including continental shelf seas and ridges whilst the darker blue areas indicate abyssal depths. (b) The area of interest (the box outlined by a yellow dotted line in panel (a)) showing contours of the rate of conversion of tidal energy (W m^{-2}), in the M2 band, from the barotropic mode. (c) The Froude number distribution in the area of interest with bottom topography overlaid (black contours representing the 100, 200 and 300m isobaths). (d) Mean profiles of buoyancy frequency (N^2) and vertical shear in the current speed (S^2) at the location of the observations. The mean is calculated for the 12 hour period of the observations. The variability is shown by envelopes which represent the 95% confidence limits estimated by bootstrapping. These profiles indicate that the Gradient Richardson number over the thermocline region is close to one, and so the thermocline is of marginal stability.

exceed the critical threshold value of 1. The phase speed c of the internal waves is found by solving the eigenvalue problem:

$$\Phi_{zz} + \frac{N^2(z)}{c_j^2}\Phi_j = 0$$
$$\Phi(-H) = \Phi(0) = 0 \tag{3}$$

where $\Phi_j(z)$ is the eigenfunction that defines the vertical structure of j-th internal mode, c_j is the phase speed of the internal mode, and $j = 1, 2, 3, \ldots$ is the mode number.

A Froude number analysis was carried out for the region, using the background stratification measured during August 2013 (Figure 1d) and the maximum velocity of the semi-diurnal M2 tide from the TPX08. The phase speed of the first internal mode for different depths was then calculated using (3). The distribution of the Froude number is shown in Figure 1c, and reveals that most of the study area, including all areas where the depth is less than 100 m, is supercritical for tidal flow and so potentially susceptible to unsteady lee-wave formation through tide-topography interaction.

3 Numerical Modelling Study

The aim of the modelling study is to show that the barotropic tidal currents are able to generate internal waves in the region of interest (i.e. poleward of the critical latitude) and to characterise the internal wave field. To achieve this we use the fully non-linear non-hydrostatic Massachusetts Institute of Technology general circulation model MITgcm [*Marshall et al.*, 1997] to simulate the tidally generated internal waves in the region.

A two-dimensional version of the model was configured with fine resolution: 1 m in the vertical and 9 m in the horizontal direction. The horizontal grid step was exponentially increased near lateral boundaries to provide non-reflectance of radiated waves from the boundaries for at least five tidal periods. Tidal forcing was applied in the model by a tidal potential added to the right hand side of the momentum balance equations. The amplitudes of the zonal and meridional velocities in tidal ellipses were set $0.3\,\mathrm{m\,s^{-1}}$ at 100 m depth. The N^2 profile was calculated from mean profiles of temperature and salinity (Figure 1d). A bank topography profile with slopes typical of those found along the transect was used. The horizontal viscosity and diffusivity were set to be constant at $0.01\,\mathrm{m^2\,s^{-1}}$, which, in conjunction with the small horizontal grid step, provided reasonable conditions for the reproduction of the details of the generation processes. A Richardson number dependent parametrization for

vertical viscosity ν and diffusivity κ, [*Pacanowski and Philander*, 1981], was used:

$$\begin{aligned} \nu &= \frac{\nu_0}{(1+\alpha Ri)^n} + \nu_b \\ \kappa &= \frac{\nu}{(1+\alpha Ri)} + \kappa_b \end{aligned} \tag{4}$$

Here Ri is the gradient Richardson number, $Ri = N^2(z)/S^2(z)$; $\nu_b = 10^{-5}\,\mathrm{m^2\,s^{-1}}$ and $\kappa_b = 10^{-5}\,\mathrm{m^2\,s^{-1}}$ are the background parameters; $\nu_0 = 1.5 \times 10^{-2}\,\mathrm{m^2\,s^{-1}}$, α=5 and n=1 are the adjustable parameters. This parameterisation increases the coefficients ν and κ in the areas where the Richardson number is small, to account for mixing processes induced by shear instability and breaking internal waves.

4 Generation mechanism

The model results show the generation of packets of high frequency waves over the topography which are initially trapped, but which propagate away as the tide slackens. The generation and the evolution of the high frequency internal wave packets over several tidal cycles is shown in Figure 2. At the beginning of the cycle (Figure 2a), the tidal flow moves across the topography and elevates the isotherms on the upstream side of the topography (identified as zone A), and depresses them on the downstream side (i.e. on the lee-side, identified as zone B). The resulting elevated and depressed features (identified as a1 and b1) are trapped whilst the flow is supercritical. As the tide weakens and the flow becomes subcritical the features, a1 and b1, are able to propagate away from the topography. The reversing tidal flow then accelerates, becoming super-critical, resulting in the generation of a second set of features (a2 and b2) which develop and are trapped as illustrated in the Hovmöller diagram (Figure 2b).

The generation process is repeated on every tidal cycle. As the features propagate they evolve into packets of high frequency internal waves radiating away from the topography as shown in Figure 2c. The Hovmöller diagram (Figure 2d) shows the evolution and propagation of the internal wave packets over a further two tidal cycles. The leading edge of the internal wave packets propagating to the left are linked by red dotted lines, with the corresponding trailing edge indicated by a black dashed line illustrating a spatial scale for the wave packet of about 5 km. The leading edge of the waves propagating to the right are linked by a dotted green line with the corresponding trailing edge again indicated by the black dotted line. The model therefore predicts that the supercritical tidal flow over the topography

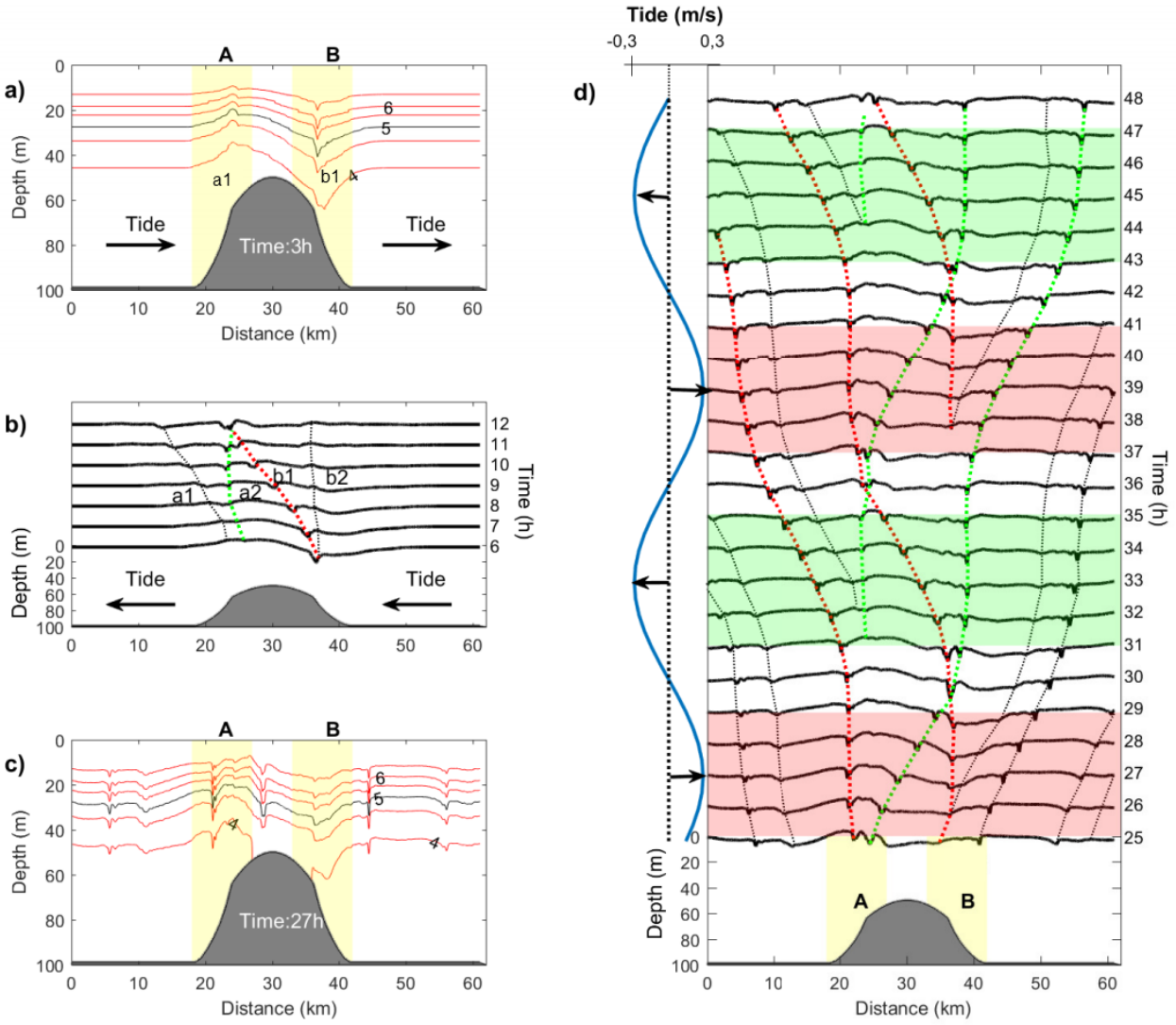

Figure 2. Simulated temperature fields (4 - 6.5 °C isotherms at 0.5 °C intervals) after (a) 3 and (c) 27 hours of model time. b) and d) The Hovmöller diagrams showing evolution of the 5° isotherm during the simulation time periods of (b) t=6-12 hours and (d) t=25-48 hours. The contour interval represents 1 hour. Green and red lines identify the features radiating away from the topography. The direction and strength of the tidal flow is shown by a blue solid line. The red and green shaded areas show time intervals with supercritical ($Fr > 1$) conditions for radiated internal waves. Generation zones A and B are shaded yellow on panels (a), (b) and (d).

generates two packets of high frequency internal waves per tidal cycle, which then radiate away. However, the wave packets propagating against the tide are held by the flow.

To illustrate characteristics of the waves from the prospective of single point measurements, we show the predicted evolution of the temperature structure at two fixed points, V1 and V2, away from the topography in Figure 3. From this prospective there is evidence of two types of waves at both locations. The first is a long-period, semi-diurnal wave which is present at both locations but smaller in amplitude at the location farthest from the topography (V2). This is consistent with linear theory which predicts the existence of only evanescent modes poleward the critical latitude.

The second type of waves evident are packets of high frequency internal waves which occur at the same point of every tidal cycle. The high frequency internal waves are present at a particular location for 3 - 5 hours during each semi-diurnal tidal cycle. These waves are characterised by a larger amplitude (approximately 10 m) wave followed by a series of smaller amplitude waves with a period of 20 - 30 minutes.

In order to determine the partitioning of tidal energy conversion between the evanescent linear tidal wave and the unsteady lee wave the model was also run for identical conditions but with the non-linear terms turned off. A comparison between the linear and non-linear cases shows that the energy transfer to non-linear internal waves accounts for 71% of the total tidal conversion. It should be noted that whilst a sensitivity analyses of the partitioning of the energy transfer between the linear and non-linear waves it beyond the scope of this paper, the ratio is likely to be very sensitive to the Froude number of the flow.

5 Observations

A 12 hour time series of velocity and turbulence profile data were collected on the edge of the bank along a short transect which approximately followed the 100 m contour. The north-south transect was repeated over two successive 6-hour periods (approximately 3 km in length) as the ship moving slowly forward. A set of microstructure observations were made using a loosely tethered Rockland VMP500 microstructure profiler (VMP) which profiled from approximately 10m below the sea surface to the sea bed. Simultaneous current profiles were taken using an RDI 300kHz acoustic Doppler current profiler (ADCP) attached to the stern of the ship, which collected data with a 2 m bin size and single ping observations every 2 seconds. The barotropic tide over this area was found to be elliptical with the ma-

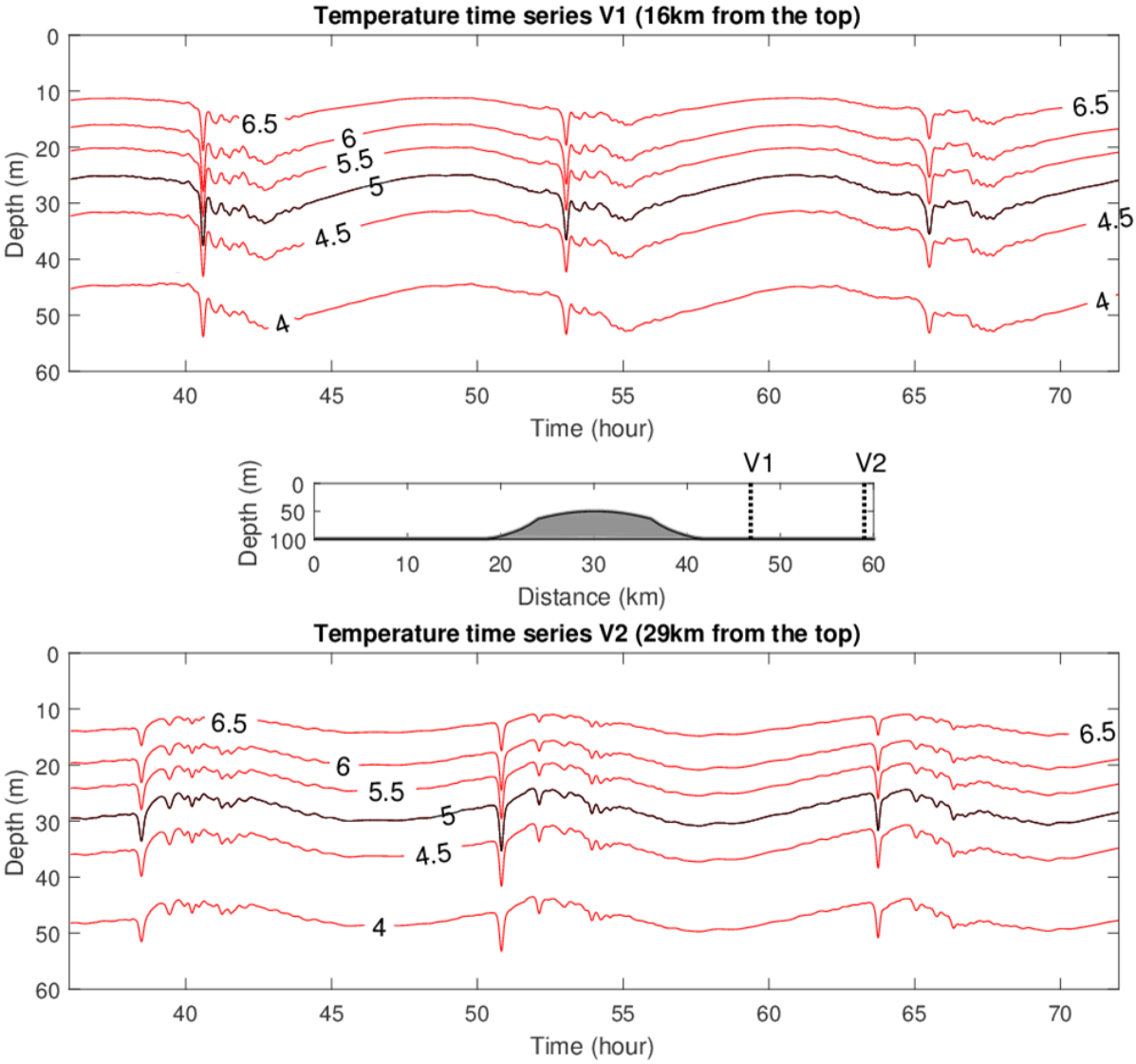

196 **Figure 3.** Temperature time series predicted by the model at two fixed points, V1 (16 km from the top of
197 the topography) and V2 (29km from the top of the topography). The positions relative to the topography are
198 shown in the middle panel. 4 - 6.5 °C isotherms are shown at 0.5 °C intervals.

jor axis oriented approximately east-west with maximum U $\sim$0.4 m s^{-1}, and the minor axis oriented approximately north-south with maximum V $\sim$0.3 m s^{-1}.

The first transect took place between 07.00 and 13.00 GMT with 41 VMP profiles collected. At this time the direction of the barotropic tide was predominantly westward, oriented approximately off-bank. The second transect took place when the flow was oriented predominantly on-bank, between 14.00 and 19.00 GMT, during which time 47 VMP profiles were collected. During both transects VMP profiles were taken approximately every 6 minutes providing profiles of temperature, salinity (and hence density) and ε [e.g. *Rippeth et al.*, 2015], with gaps during the first transect and between the first and second transects whilst the ship repositioned.

Mean profiles show that the gradient Richardson number is approximately 1, indicating the water column is susceptible to shear instability (Figure 1d). The time series of temperature, ε and the observed mid-water currents are presented together with the shear in the horizontal velocities across the thermocline, in figure 4. During the first transect the thermocline is relatively thin, widening from 10 to 20 m when defined by the 4.5 and 6°C isotherms. There are intermittent displacements in the isotherms of up to 15 m with periods of 20 - 30 minutes. These features are particularly apparent from about 09:00 to the gap in the data after 10:00, and again around 12:00.

During the second transect the thermocline again thickens, with the separation of the 4.5 and 6°C isotherms increasing from 15 to 30 m over the duration of the transect. From about 15.00 hours to the end of the time series there are seven internal waves evident, with the amplitude of the leading wave about 15 m, and the following waves about 5 - 10m. The period of the waves is approximately 30 minutes. Estimates of shear in the horizontal velocities, across the thermocline (Figure 4b), indicate variability of up to an order of magnitude, with the peaks in shear occurring approximately every 30 minutes, and so correlated with the vertical movement of the isotherms associated with the presence of internal waves.

A time series of the vertical distribution of the ε is shown in Figure 4(c). High values of ε are evident close to the the boundaries, and in particular in the bottom boundary layer. Within the thermocline there is high temporal variability in ε with isolated patches of enhanced dissipation, which coincide with the periods of significant internal wave activity. The mean thermocline ε over the period of the second transect, is 4.5×10^{-5} W m^{-3} with several periods of significant enhancement evident (e.g. around 15:00 and 16:00 coincident

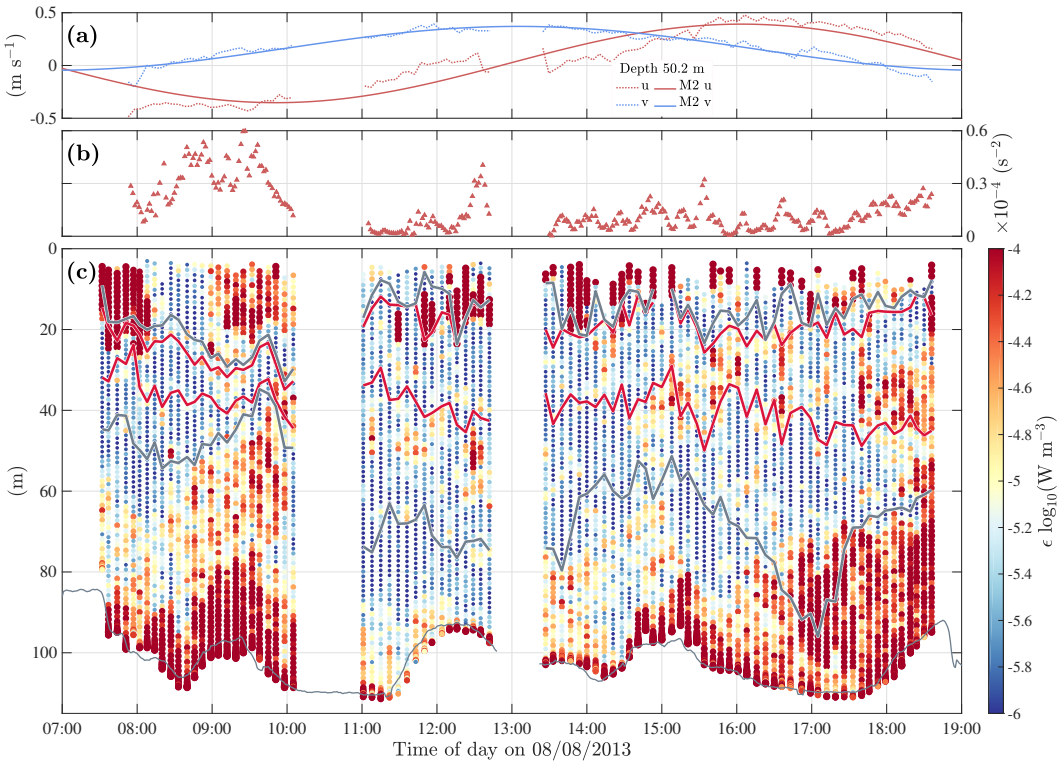

Figure 4. (a) Observed velocity (dotted line) together with the tidal current velocity predicted through tidal analysis (solid line) in the eastward (red - approximately on-bank) and northerly (blue) directions at a mid-depth location (50 m). (b) Vertical shear in the horizontal velocity across the thermocline evaluated between 10 m depth-averages centred around 8.15 m and 68.15 m with 240 sec running average at 100 sec intervals based on raw observations at 2 s intervals and 2 m depth bins. (c) The coloured dots represent measurements of ε from VMP profiles taken approximately every 6 minutes; the red lines are the 4.5 and 6°C isotherms; and the grey lines indicate the surface mixed layer (SML) and bottom boundary layer (BBL) based on a maximum temperature difference of 0.4°C from the boundary value, with ε values between the grey lines indicating dissipation within the thermocline.

with isotherm displacements of up to 15 m and spikes in the shear) and towards the end of the transect. Water column integrated estimates of dissipation imply that the total dissipation is dominated by bottom boundary layer dissipation, although the total observed dissipation in the thermocline (i.e. between the bottom boundary layer and the surface mixed layer) accounted for 37% (bootstrap 95% confidence limits of 28 to 49%) of the dissipation observed below the surface mixed layer.

6 Discussion

Recent observations have shown continental shelf break regions of the Arctic Ocean host significant barotropic tidal energy conversion [*Rippeth et al.*, 2015], with evidence of greatly enhanced ε , and by implication mixing, over sloping topography in the presence of significant tides [e.g. *Padman and Dillon*, 1991; *D'Asaro and Morison*, 1992; *Rainville and Winsor*, 2008; *Fer et al.*, 2010; *Rippeth et al.*, 2015]. This is in sharp contrast to much of the central Arctic Ocean which is found to be remarkably quiescent [e.g. *Lincoln et al.*, 2016; *Shibley et al.*, 2017]. However, much of the Arctic Ocean lies poleward of the critical latitude and so the conversion of barotropic tidal energy to a freely propagating linear internal tide, over sloping topography, is suppressed by rotation.

In this paper we present a mechanism for tidal energy conversion poleward of the critical latitude, in which supercritical tidal flows result in the transfer of energy to short length-scale internal lee waves which are generated over steep topography as a result of strong non-linear advection. The mechanism is demonstrated through a high resolution non-linear numerical modelling study focused on a region of sloping topography in the vicinity of the Spitsbergen Bank, an area identified as hosting significant barotropic tidal conversion, and where the tidal flow is supercritical (Fr $>$ 1). The modelling study predicts that for the conditions found in this area at this time approximately 71% of the barotropic tidal energy converted to baroclinic modes is associated with the non-linear internal waves whilst the remainder is associated with an evanescent semi-diurnal internal tide. It is worth noting that the non-linear wave component is not currently included in the tidal mixing parameterisation [*Falahat and Nycander*, 2015] available for application in locations poleward of the critical latitude.

A 12 hour time series of temperature and velocity profiles collected on the edge of the Spitsbergen Bank reveal the presence of high frequency internal waves with coincident en-

hancement of shear and characteristics similar to those predicted by the model. Coincident ε profiles reveal that water column integrated dissipation is dominated by dissipation close to the boundaries, with the tidally generated bottom boundary layer accounting over half of the observed ε. This would suggest that a significant proportion of the converted tidal energy is dissipated within the well mixed bottom boundary layer and so not available to support mixing. Approximately a third of the observed ε occurs within the stratified mid-water column and so will potentially contribute to mixing.

The observed thermocline mean ε is comparable to those previously reported over the continental shelf break to the north of Svalbard [e.g. *Rippeth et al.*, 2015] and are similar to those reported over sloping topography for regions of similar water depths and tidal currents, equatorward of the critical latitude [e.g. *Rippeth*, 2005]. Whilst the high spatial and temporal variability of dissipation, and therefore mixing, associated with the lee-wave energy transfer mechanism evident from the modelling study, imply that the resolution of the observations reported here fails to fully resolve the associated mixing, they do indicate the potential of this mechanism to contribute to mixing. Evidence of the spatial extent of this energy conversion mechanism comes from recent studies based on Envisat synthetic aperture radar images which show the existence of high frequency internal waves across large areas of the eastern Arctic [*Kozlov et al.*, 2014, 2015].

The analysis presented highlights that the barotropic tidal conversion alone is not a good estimator of mixing for a number of reasons. The partitioning of converted energy between the evanescent internal tide and the non-linear internal waves will vary considerably according to local flow conditions. Furthermore, the proportion of the converted energy dissipated in the bottom boundary layer (and so not available to mix the water column) is also likely to vary greatly. However, the Froude number may be a useful diagnostic in the prediction of the location and evolution of mixing hot spots poleward of the critical latitude. Accordingly changes in both stratification and flow over topography could result in the development of supercritical flow, and consequently mixing, as reported for lower latitudes [*Stephenson et al.*, 2015]. There are large seasonal changes in the stratification in the Arctic. Furthermore there is evidence of increased currents associated with sea ice loss [*Giles et al.*, 2012]. These changes will impact both the tidal conversion rate and the partitioning of energy between the linear and non-linear modes and so lead to variations in both the magnitude of, and spatial and temporal patterns in, tidally driven mid-water column mixing.

Acknowledgments

TPR, VV and NS contributed equally to the writing of this paper. Data collection and analysis by BJL and TPR was funded through the UK NERC TEA-COSI Consortium (PI: SB, NE/I028947/1). BDS is supported by NERC award 1500369 through the Envision DTP. JAMG acknowledges NERC funding from FASTNEt (NE/I030224/1) and RidgeMix (NE/L004216/1). We thank the officers, crew and principal scientist of the RRS James Clark Ross cruise 288, supported by the NERC ACCACIA consortium. TPR and BJL planned the field work whilst BJL lead the data collection. JAMG, BJL and BDS all contributed to data analysis. VV and NS carried out the numerical modelling.

The observations reported in this paper are available on request from British Oceanographic Data Centre, National Oceanography Centre, Liverpool (http://www.bodc.ac.uk).

References

Bell, T.H. (1975) Lee waves in stratified flows with simple harmonic time dependence. *J. Fluid Mech.*, *67 (4)*, 705–722.

D'Asaro, E.A., and J. H. Morison (1992) Internal waves and mixing in the Arctic Ocean. *Deep Sea Res. II*, *39*, 459-484.

Egbert, G.D., and R.D. Ray (2001) Estimates of M2 tidal energy dissipation from TOPEX/Poseidon altimeter data, *J. Geophys. Res.*, 106(10), 22475–22502.

Falahat, S., and J. Nycander (2015) On the Generation of Bottom-Trapped Internal Tides, *J. Phys. Ocean.*, 45, 526–545.

Fer, I., R. Skogseth, and Geyer (2010). Internal waves and mixing in the Marginal Ice Zone near Yermak Plateau. *J. Phys. Oceanogr.*, *40(7)*, 1613-1630.

Giles, K.A., S.W. Laxon, A.L. Ridout, D.J. Wingham and S. Bacon (2012). Western Arctic Ocean Freshwater storage increased by wind-driven spin-up of the Beauford Gyre. *Nat Geosci*, *5*, 194-197, doi:10.1038/ngeo1379.

Green, J.A.M., and J. Nycander (2013). A comparison of tidal conversion parameterization for tidal models. *J. Phys. Oceanogr.*, *43*, 104-119.

Kozlov, I., D. Romanenkov, A. Zimin, B. Chapron (2014) SAR observing large-scale nonlinear internal waves in the White Sea, *Rem. Sensing of Envir. 147*, 99-107.

Kozlov, I., V. Kudryavtsev, E. Zubkova, O. Atadzhanova, A. Zimin, D. Romanenkov, A. Myasoedov, and B. Chapron (2015) SAR observations of internal waves in the Russian

Arctic Seas, *Proc. IGAARS Symposium*, 947-949.

Lincoln, B.J., T.P. Rippeth, Y.-D. Lenn, M.L. Timmermans, W.J. Williams, and S. Bacon (2016). Wind-driven mixing at intermediate depths in an ice free Arctic Ocean. *Geophys. Res. Lett.*, *43*, doi:10.1002/2016GL070454

Marshall, J., A. Adcroft, C. Hill, L. Perelman, and C. Heisey (1997), A finite-volume, incompressible Navier-Stokes model for studies of the ocean on the parallel computers, *J. Geophys. Res.*, 102, 5733–5752.

Munk, W.H., and C. Wunsch (1998) Abyssal recipe II: Energetics of tidal and wind mixing. *Deep-Sea Res. I*, *45*, 1977-2010.

Nakamura, T., and T. Awaji (2000) The growth mechanism for topographic internal waves generated by an oscillatory flow, *J. of Phys. Oceanorg.*, *31*, 2511-2524.

Nakamura, T., T. Awaji, T. Hatayame, K. Akimoto, T. Takizawa, T. Kono, Y. Kawasaki, and M. Fukasawa (2000) The generation of large-amplitude unsteady lee waves by subinertial K1 tidal flow: a possible vertical mixing mechanism in the Kuril Straits, *J. of Phys. Oceanorg.*, *30*, 1601-1621.

Nycander, J. (2005) Generation of internal waves in the deep ocean by tides, *J. Geophys. Re.*, *110*, C10028.

Pacanowski, R.C., and S. G. H. Philander (1981) Parameterisation of vertical mixing in numerical models of Tropical Oceans, *J. Phys. Oceanogr.*, *11*, 1443-1451.

Padman, L., and T.M. Dillon (1991) Turbulent mixing near Yermak Plateau during the Coordinated Eastern Arctic Experiment. *J. Geophys. Res.*, *96*, 4769-4782.

Padman, L., and S. Erofeeva (2004) A barotropic inverse tidal model for the Arctic Ocean. *Geophys. Res. Lett.*, *31*, L02303.

Rainville, L., and P. Winsor (2008) Mixing across the Arctic Ocean: microstructure observations during the Beringia 2005 expedition. *Geophys. Res. Lett.*, *35(8)*, L08606, doi:10.1029/2008GL033532.

Rippeth, T.P. (2002). Mixing in seasonally stratified shelf seas: a shifting paradigm. *Phil. Trans. R. Soc. A*, *363*, 2837-2854, doi: 10.1098/rsta.2005.1662.

Rippeth, T.P., B.J. Lincoln, Y.-D. Lenn, J.A.M. Green, A. Sundfjord, and S. Bacon (2015) Tide-mediated warming of Arctic halocline by Atlantic heat fluxes over rough topography, *Nature Geoscience*, *8*, 191-194.

Shibley, N.C., M.L. Timmermans, J.R. Carpenter, and J.M. Toole (2017). Spatial variability of the Arctic Ocean's double-diffusive staircase. *J. Geophys. Res.*, *122(2)*, 980-994, DOI:

389 10.1002/2016JC012419

390 Stephenson, G. R., J. E. Hopkins, J. A. M. Green, M.E. Inall and M.R. Palmer (2015) WInd-
391 mixing by storms modifies baroclinic energy flux on the Celtic Sea shelf. *Geophys. Res.*
392 *Letts*, doi: 10.1002/2014GL062627.

393 Vlasenko V., N. Stashchuk, K. Hutter, and K. D. Sabinin (2003), Nonlinear internal waves
394 forced by tides near the critical latitude, *Deep Sea Res. I*, *50*, 317-338.

395 Vlasenko V., N. Stashchuk, and K. Hutter (2005), Baroclinic tides: theoretical modeling and
396 observational evidence. Cambridge University Press. 365 pp.